applied optics

Ultraviolet (250–550 nm) absorption spectrum of pure water

John D. Mason,[1] Michael T. Cone,[2] and Edward S. Fry[1,*]

[1]Department of Physics & Astronomy, Texas A&M University, 4242 TAMU, College Station, Texas 77843, USA
[2]Department of Physics & Astronomy, Rice University, 6100 Main Street, Houston, Texas 77005, USA
*Corresponding author: fry@physics.tamu.edu

Received 7 June 2016; accepted 4 August 2016; posted 8 August 2016 (Doc. ID 267634); published 31 August 2016

Data for the spectral light absorption of pure water from 250 to 550 nm have been obtained using an integrating cavity made from a newly developed diffuse reflector with a very high UV reflectivity. The data provide the first scattering-independent measurements of absorption coefficients in the spectral gap between well-established literature values for the absorption coefficients in the visible (>400 nm) and UV (<200 nm). A minimum in the absorption coefficient has been observed in the UV at 344 nm; the value is $0.000811 \pm 0.000227\ m^{-1}$.

OCIS codes: (300.1030) Absorption; (300.6540) Spectroscopy, ultraviolet; (010.4450) Oceanic optics; (010.1030) Absorption.

http://dx.doi.org/10.1364/AO.55.007163

1. INTRODUCTION

Volume light absorption is an inherent optical property of pure water; together with scattering and the optical characteristics of other dissolved/suspended materials, they give large bodies of water their apparent color [1,2,3]. For example, the main reason a large body of pure water appears blue/violet is because (i) the absorption of blue light is low, and thus, more blue light is available for scattering out of the water [1,4], and (ii) Rayleigh scattering is much more effective at scattering shorter than longer wavelengths out of the water.

Much as in the terrestrial food web, energy from the sun strongly influences the aquatic food web. Organisms, such as phytoplankton, convert radiation from the sun into usable energy through photosynthesis [5]. Because of the low optical absorption of water in the blue, the many pigments in phytoplankton (e.g., chlorophyll) evolved so as to strongly absorb blue–green light, leading to an ideal habitat for phytoplankton [2,6].

While the visible and infrared absorption spectrum of pure liquid water has been relatively well established (>400 nm) [7–10], agreement on the absorption spectrum of water in the ultraviolet, as well as in portions of the blue, has yet to be achieved [8,11,12]. The ultraviolet spectrum of water is impacted by many factors, such as organic content and dissolved oxygen, which are independent of the intrinsic optical properties of pure water. The most commonly accepted studies of the UV properties of pure water are from Quickenden and Irvin 11, Ghormley and Hochanadel 13, and Kröckel and Schmidt [14], which focus on the spectral region of 180–320 nm. In each of these studies, the attenuation (scattering and absorption) was measured. The absorption was then calculated by subtracting the molecular scattering (Rayleigh scattering) from the measured attenuation. In particular, the studies by Kröckel and Schmidt and by Quickenden and Irvin both used the same differential attenuation experimental design. While the measured attenuation was identical in both studies, the scattering contributions used by Kröckel and Schmidt varied from a factor of 2.2 lower at 190 nm to 2.6 lower at 320 nm than the scattering contributions used by Quickenden and Irvin. Therefore, the resulting absorption coefficients are quite different for the two studies [11,14].

The above example demonstrates the need for a scattering-independent measurement. Since Rayleigh scattering is proportional to λ^{-4}, scattered light rapidly increases for shorter wavelengths. In the marque book by Jonasz and Fournier (2007), *Light Scattering by Particles in Water: Theoretical and Experimental Foundations*, the authors state that "the results are particularly sensitive to [intrinsic scattering corrections]… where the absorption of water is at a minimum." This scattering correction is especially problematic in the UV where scattering grows increasingly large. Jonaz and Fournier continue by stating that "the minimum absorption of water could be considerably smaller [than the literature values at 420 nm], and the level of sensitivity and accuracy required to carry out an accurate absorption experiment…is still daunting today. The most promising approach so far appears to be the integrating cavity absorption meter [(ICAM)] in combination with improved water purification systems" [3]. The present study combines a state-of-the-art water purification system capable of producing semiconductor-grade water with the improved

sensitivity and scattering independence of a new version of the ICAM. The ICAM instrumentation concept previously used provided reliable water absorption data for visible wavelengths. The new ICAM was designed to provide a reliable UV absorption spectrum down to 250 nm [8,15].

In 1992, Fry *et al.* developed the ICAM to measure the absorption coefficient of weakly absorbing materials independent of scattering [15]. As a result of the multiple passes through the sample due to the diffuse reflections from the walls of the ICAM cavity, the ICAM dramatically increases the optical path length through a weakly absorbing sample. This increased path length through the sample significantly improves the measurement. Pope and Fry used an ICAM made from the diffuse reflecting material Spectralon to characterize the absorption structure of water from 380 to 700 nm [8,16]. The visible spectrum of water was independently verified by Sogandares and Fry using photothermal deflection spectroscopy [9]. The data from Pope and Fry showed a minimum absorption of 0.0044 m^{-1} at 418 nm. While the high reflectivity of Spectralon creates a long path length in the visible (~10 m), Spectralon's reflectivity diminishes for shorter wavelengths (UV) resulting in a decrease of the instrument sensitivity for these wavelengths [15].

More recent results indicate that the Pope and Fry data overestimate the absorption from water between 380 and 440 nm where the Spectralon begins to absorb. In 2007, Morel *et al.* characterized the optical properties of the "clearest" natural waters from 300 to 500 nm using hyperspectral irradiance: they theorized that the absorption of pure water might be lower than previously hypothesized between 300 and 400 nm. Morel *et al.* applied a smooth extrapolation for the data gap between 320 nm (Quickenden and Irvin) and 420 nm (Pope and Fry) [17]. The extrapolated data was significantly lower than the Pope and Fry data from 380 to 420 nm. It is important to recognize that Morel's values between 320 and 420 nm are an extrapolation from previous literature and do not represent experimental data. However, it highlights the importance of performing high quality water absorption measurements in this region.

In 2009, Cruz *et al.* measured the absorption of pure water using an ultrasensitive thermal lens spectroscopy technique similar to the technique used in the work by Sogandares and co-workers [9,10]. They measured the absorption spectrum of pure water at three points in the ultraviolet (351, 364, and 406) and several points in the visible. Their data agrees with the Pope and Fry data for $\lambda > 420$ nm; however, it demonstrates a lower minimum near 364 nm that is more than a factor of 3 smaller than the previously established minimum. Because Cruz *et al.* measured only a few points in the ultraviolet region that disagree with many of the established results, their results have been met with initial skepticism. An independent method of verification could properly evaluate these results.

In 2015, Cone *et al.* characterized a new diffuse reflecting material, fumed silica. Fumed silica has been shown to have a much higher diffuse reflectivity ρ than Spectralon; see Table 1.

The higher ultraviolet reflectivity of fumed silica cavities generates increased path lengths comparable to the path lengths of visible light in cavities made from Spectralon; consequently, measurements with higher sensitivity are possible [19,20]. By implementing the fumed silica diffuse reflector in the ICAM design, a new instrument, ICAM-II, was created that had an improved sensitivity capable of measuring the absorption spectrum of water in the UV. The path length at 532 nm in this ICAM-II is ~24 m.

Table 1. Reflectivities of Fumed Silica [18] and Spectralon [16]

	$\lambda = 532$ nm	$\lambda = 266$ nm
Fumed silica (%)	99.92	99.69
Spectralon (%)	99.8	96

The ICAM-II was used to measure the absorption spectrum of pure water in the 250–550 nm wavelength region. The results show that the absorption of pure water is actually lower in the 300–400 nm region than the previously accepted minimum values at 418 nm. These measurements agree favorably with the accepted values of Pope and Fry from 440 to 550 nm as well as the Rayleigh-corrected results from Quickenden and Irvin for 250–300 nm [8,11].

2. NEW DIFFUSE REFLECTOR

Aerosil EG50 fumed silica from Evonik Degussa was used. A detailed discussion of the powder can be found in Cone *et al.* [18]. The powder was baked to remove moisture using a Fischer Scientific Isotemp Vacuum Oven that was pumped by a liquid nitrogen sorption pump. The oven temperature was set to ≈280°C while a vacuum of ≈1 Torr was established. The oven was then backfilled with ultra-high-purity argon while the loose powder was cooling. The baked powder was first pressed under a hydraulic press to ≈100 psi, forming a semi-solid disc. This disc was then masticated and stirred until a coarse powder was created. This coarse powder was then hand-pressed to form the ICAM-II cavities.

Basically, when the powder was pressed at 100 psi and masticated, the resulting coarse powder consisted of irregularly shaped interlocking agglomerate particles that were formed from the original particles. Since the integrating cavities of the ICAM-II had to be hand-pressed to avoid damaging the fused silica components, the prepacking created tighter interlocking interfaces than is possible by hand-pressing. Many of the tightly packed interlocked pieces from the hydraulic press remained and provided a higher density of powder in the hand-pressed walls of the ICAM-II integrating cavities.

3. ICAM-II

Previous versions of the ICAM have been discussed in detail [8,15]. A block diagram of the ICAM system is presented in Fig. 1 as an overview.

The light source was a 150-W ozone-free xenon arc lamp which emits a broadband spectrum. A 3-inch steel Oriel liquid filter (Oriel 6227) was used to significantly reduce NIR radiation and thereby minimize heating of downstream optics. The filter was manufactured with fused silica windows to allow transmission of ultraviolet wavelengths down to 250 nm. It was filled with distilled water and held at a constant temperature

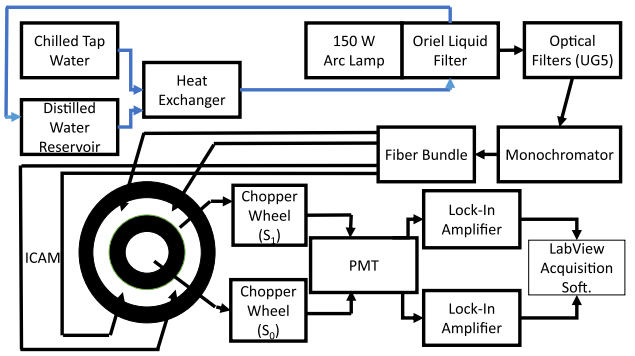

Fig. 1. Block diagram of the experimental setup for the ICAM.

using a heat exchanger connected to a chilled tap water line. A 2-mm-thick UG5 glass filter from Schott glass was used to further remove NIR and visible radiation before final wavelength selection. Final wavelength selection was achieved using a CVI Digikrom 240 monochromator. The monochromater was fitted with UV-grade fused silica optics and contained a reversible two-grating mount with peak transmissions at 500 and 330 nm. Tuning of the monochromater was controlled by a computer through a GPIB interface. The monochromater bandwidth is 1.8 nm with a slit width of 600 μm; it is 6 nm with a slit width of 2000 μm. A 45-mm-diameter camera shutter was attached to the opening of the monochromater. The shutter can be closed to verify that background effects are eliminated. The system was enclosed in a wooden box to shield the aperture from dust and ambient light. A custom fiber array of eight 600-μm-diameter silica-core fibers with silica cladding were arranged linearly in front of the exit slit of the monochromator to collect light and deliver it to the integrating cavity.

Cross sections of the ICAM-II are shown in Fig. 2. It consists of two concentric integrating cavities centered around a quartz glass sample cell. Light is injected into the outer cavity (air gap) and diffuses through the inner cavity wall to the sample region. The quartz cell has an inlet and outlet port located at the top and bottom of the assembly.

The outer integrating cavity was constructed by placing a 20.6-cm-diameter fused silica tube, Q1, ($h = 26.0$ cm) centered inside a piece of 25.4-cm-diameter Schedule 40 PVC Pipe ($h = 33$ cm). A special jig was used to ensure that Q1 is centered (x, y, and z) inside the PVC. The area between the PVC and Q1 was packed rigorously with the previously prepared powder (see Section 2) using several hand tools. The reflectivity of the outer cavity wall is important as it minimizes loss of light from the instrument by diffusion through the wall. A second fused silica cylinder, Q2, with diameter of 16 cm ($h = 15.85$ cm) was centered inside of Q1. The region between Q1 and Q2 was left empty to serve as a reference cavity and optical injection site. A 1.538-L cylindrical quartz sample cell with two quartz stems was centered inside of Q2. The area between Q2 and the quartz sample cell was lightly filled with the fumed silica powder to form the outer wall of the inner cavity and the inner wall of the outer cavity. If this region is packed too tightly, the reflectivity of the wall would be too high to obtain a measurable amount of light in the sample region. An alternate approach is to reduce the thickness of the inner cavity wall. The sample region surrounded by quartz powder comprises the inner cavity. Light exiting the monochromater was injected into the reference (outer) cavity through the eight quartz fibers. Eight small sections of hypodermic tubing encased in Spectralon are used to pass the quartz fibers through the top and bottom of the outer cavity wall and into the reference cavity. Four of the quartz fibers are equally spaced at 90° intervals around the top cap and four around the bottom cap.

A diagram of the detection scheme has been shown in Fig. 3. The irradiances from the inner cavity wall (S_0) and from the outer cavity wall (S_1) were sampled through two optically polished 6-mm- and 5-mm-diameter quartz rods. A larger quartz rod was chosen for the inner cavity to increase the signal from the weaker intensity light. The signal from each rod was passed through separate optical chopper wheels. The quartz rods were placed as close to a chopper blade as possible such that the rod

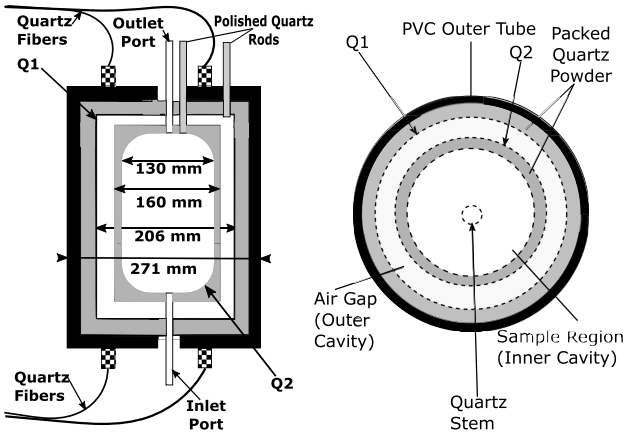

Fig. 2. Vertical (left) and horizontal (right) cross section of the ICAM-II.

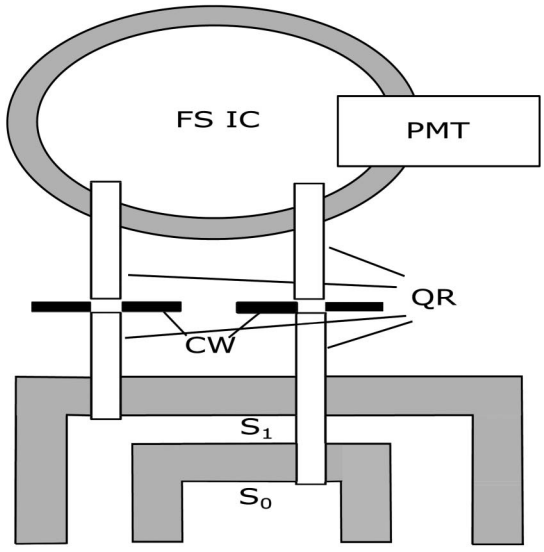

Fig. 3. Diagram of the detection system: PMT is the photomultiplier tube, FS IC is a fumed silica integrating cavity, QR are quartz rods, CW are the chopper wheels, S_1 is the signal from the outer cavity, and S_0 is the signal from the inner cavity.

did not hit the blade. The chopper wheel frequencies were set to 1.552 and 1.207 kHz. An identical rod was placed on the opposite side of each chopper wheel to collect the light emitted by the first rod and deliver it to a second fumed silica integrating cavity that is monitored by a quartz-windowed photomultiplier tube (PMT), 9813QB ET Enterprises. The spectral response of the latter was 160–630 nm [21].

The PMT signal was coupled into a pair of Stanford Research Systems Model SR 830 Lock-in Amplifiers (LIAs). The frequency from each chopper wheel was provided as a reference to the LIA that measured the corresponding S_0 or S_1. A ratio of the signals from the LIAs was taken (S_1/S_0) and recorded using a LabView Visual Interface (VI). By referencing the signal from the inner cavity to the outer cavity with a single detector, intensity fluctuations from the light source as well as thermal fluctuations from the PMT were eliminated as sources of noise.

Data acquisition, instrument control, and signal processing and analysis were accomplished using LabView software. A sample response function (S_1/S_0) for an empty cavity is shown in Fig. 4.

A. Theoretical Background

The ICAM signal is related to the absorption of the sample by

$$\frac{S_1}{S_0} = S = \frac{4}{C_1}\alpha V + C_0', \tag{1}$$

where S is the ratio of the signal from the outer cavity to the signal from the inner cavity (S_1/S_0), α is the absorption coefficient of the sample, V is the volume of the sample region, and C_0' and C_1 are constants that account for fiber and detector spectral responses, as well as variable wavelength behavior of the quartz powder [8,15]. Solving for the absorption coefficient, α, yields

$$\alpha = \frac{C_1}{4V}(S - C_0'). \tag{2}$$

We consider the two partial derivatives from the above relations. From Eqs. (1) and (2), we have

$$\left.\frac{\partial S}{\partial V}\right|_{\alpha} = \frac{4}{C_1}\alpha, \tag{3}$$

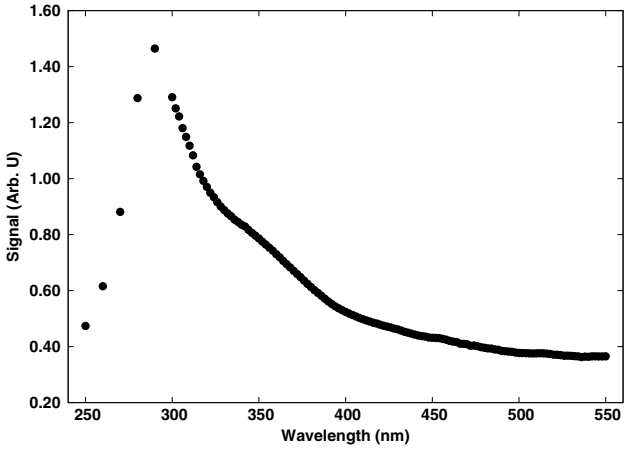

Fig. 4. Response function of a single ICAM-II scan.

and

$$\left.\frac{\partial \alpha}{\partial S}\right|_{V} = \frac{C_1}{4V}. \tag{4}$$

Multiplying Eq. (3) with Eq. (4) and solving for α, we have

$$\alpha = V\left.\frac{\partial S}{\partial V}\right|_{\alpha}\left.\frac{\partial \alpha}{\partial S}\right|_{V}. \tag{5}$$

Thus, the absorption coefficient can be obtained by measuring the cavity response as a function of a changing volume, $\frac{\partial S}{\partial V}|_{\alpha}$, for your desired sample as well as the response for a set of samples with known absorption coefficients, $\frac{\partial \alpha}{\partial S}|_{V}$. We will detail each of these measurements in the following two sections.

B. Determination of the ICAM-II Volume Response for Water ($\partial S/\partial V$)

The volume response for water involves measuring the signal from the ICAM-II for several different volumes of ultra-high-purity (UHP) water. UHP water was obtained by first purifying tap water using an EMD Millipore Rios/Elix reverse osmosis (RO) system. The output resistivity of the water from this system was measured at roughly 12–15 MΩ · cm. The water was delivered from the RO system to a sealed 60-L nalgene container. A vent filter cap was attached to the top of the nalgene to prevent atmospheric contamination. Immediately before use, this water was first passed through an EMD Millipore Milli-Q A10 UV system where water quality was monitored for total organic carbon (TOC). The Milli-Q system includes an electro-deionization system, a UV-oxidation lamp, and an ultrafiltration filter. It was then passed through a 0.22-μm polishing filter immediately before dispensing. The resulting water for this study had a resistivity of 18.2 MΩ · cm and a TOC level of 4–5 ppb.

It has been well documented that Quickenden and Irvin had gone through painstaking efforts to remove dissolved oxygen from their water sample, which has been shown to absorb strongly in the UV [11]. In 2014, Kröckel and Schmidt were able to reproduce the attenuation results from the Quickenden and Irvin study. Kröckel and Schmidt used a similar water system to the one used in this study. They noted that an additional cleaning step using a double-quartz distillation under a pure nitrogen atmosphere did not impact the study [14]. A possible explanation for why the cleaning step has no impact is that the UV-oxidation lamp converts dissolved oxygen into ozone. That ozone oxidizes trace elements in the water that are removed through the ultrafiltration filter. Consequently, the amount of dissolved oxygen in the final sample would be reduced [22].

To verify that this observation by Kröckel and Schmidt was consistent with our Milli-Q system, separate samples were measured after being bubbled under two different high-purity gas environments for 40 min separately, UHP nitrogen and UHP argon. Butler *et al.* showed that additional bubbling after 40 min had no tangible effect on the dissolved oxygen content [23]. This additional purification step also had no discernible impact on our absorption spectrum.

Since ultra-pure water leaches material from anything that it contacts, the system for delivery and storage for water leaving the EMD Millipore commercial device was made mainly from fused silica [24]. Fused silica was selected for its low leaching

characteristics while in contact with water. A schematic of the water delivery system is shown in Fig. 5. High-purity water was stored in a 6-cm-diameter, 1.5-m-long quartz reservoir that was tapered at the top and bottom to a 5-mm inner diameter (ID) stem. Water was delivered to the reservoir via low-leaching Tygon tubing with a quartz valve attachment. The Tygon tubing was purged of stagnant water by running the high-purity water through the tubing for ∼2 min. This water was immediately discarded. After purging the line, the valve attachment was connected to a quartz tee using a bare quartz ball-and-socket joint located at the bottom taper of the reservoir. One end of the tee is connected to the reservoir while the other is connected directly to the sample cell of the ICAM-II via a 5-mm ID quartz tube. Once the reservoir was filled, the valve was closed to isolate the water in the reservoir from the Tygon tubing.

The top taper of this reservoir was connected to a UHP nitrogen line. The nitrogen line contained a release valve to reduce air pressure above the water in the reservoir. Conversely, the pressure above the water was increased by filling the region with nitrogen from a UHP nitrogen canister. Raising the pressure above the water "pushes" the water through the delivery tube and into the sample region of the ICAM-II. By raising and lowering the pressure above the water in the vessel, the water level inside of the ICAM-II was precisely controlled.

The volume of water in the ICAM was monitored by measuring the height of the water in the quartz reservoir relative to the height of the initial filling.

To measure the volume response, water was first filled to the base of the ICAM-II. The volume of water in the sample cell was increased in increments of ∼150 mL for each measurement. At each increment, S was measured 100 times and averaged at each wavelength over the desired range. $S(V)$ was determined by measuring S for at least ten different volumes. A least-squares fit was performed at each wavelength to find $\partial S \backslash \partial V$. Several of these fits are shown in Fig. 6. Note, as evident in Fig. 6, $\partial S \backslash \partial V$ is proportional to the absorption coefficient, α, divided by the wavelength dependent factor, C_1 [i.e., Eq. (3)].

The slope of the volume response for pure water is shown in Fig. 7. A step size of 10 nm was chosen for wavelengths below 300 nm to allow for a larger monochromater slit width

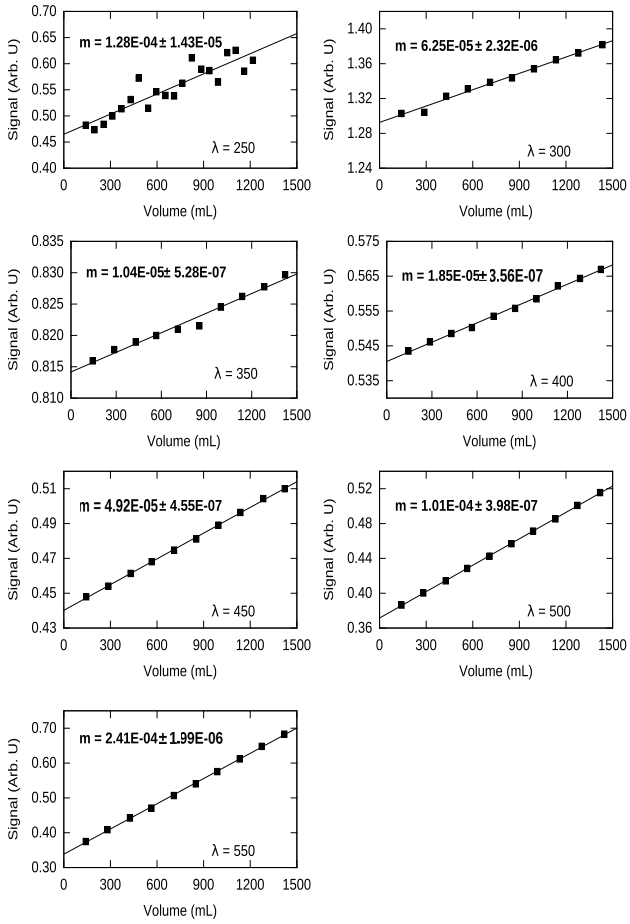

Fig. 6. Sample of the measurement of the ICAM-II signal as a function of volume. A least-squares fit is applied to each wavelength to obtain the slope.

(2000 μm). This facilitates illumination in the ICAM-II in a region where the lamp output diminishes.

It is important to note that the experimental procedure used in this study varies slightly from the original Pope and Fry study. They first made a measurement with the sample region

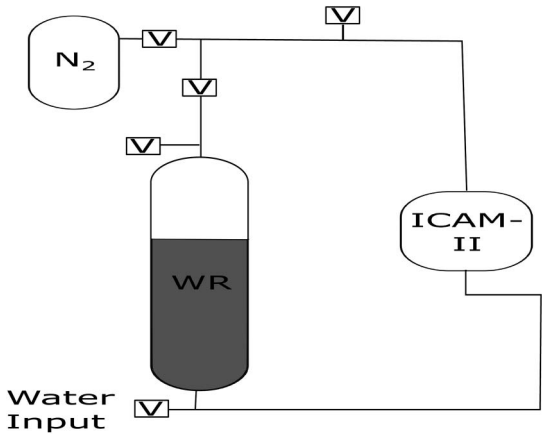

Fig. 5. Diagram of the pure water delivery system: WR is the water reservoir, V are valves, and N_2 is the UHP nitrogen canister.

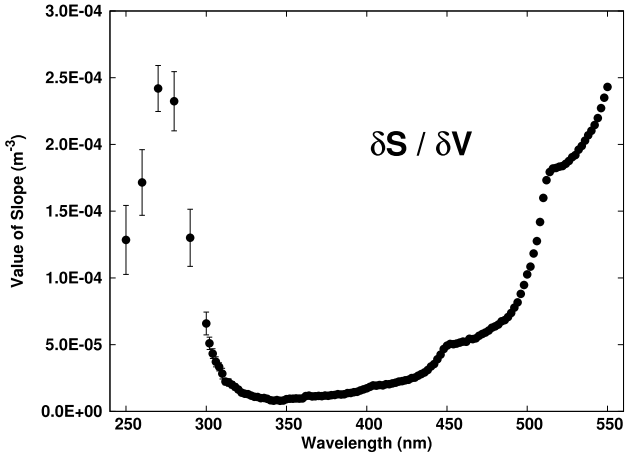

Fig. 7. Measurement of the slopes of the ICAM-II volume response for water as a function of wavelength.

completely filled. An empty cavity measurement was subtracted from the full cavity measurement. The instrument was finally calibrated by measuring the ICAM response to incrementally increasing volumes of pure water (the same procedure as outlined above) and measuring the ICAM signal as a function of increasing absorption for several reference samples (see the following section). In the Pope and Fry method, the subtracted signal (full minus empty) serves as the basis for the water absorption measurement. In contrast, the ICAM-II does not involve a signal detector at the point where the cavity is half-filled. Consequently, it just uses the instrument response to a changing volume as the raw uncalibrated data. This subtle change in methodology significantly simplifies the analysis.

C. Determination of ICAM-II Absorption Response ($\partial\alpha/\partial S$)

The determination of $\partial\alpha/\partial S$ was accomplished by measuring the cavity response to reference samples with accurately known absorption coefficients. Irgalan Black was chosen because of (1) its lack of fluorescent response in the UV, (2) its large UV absorption cross section, and (3) its previous success in ICAM experiments [8]. The lack of fluorescent response of the dye was verified by irradiating a concentrated sample of dye with the fourth harmonic of an Nd:YAG (266 nm) and measuring the sample radiance with a spectrometer.

For the calibration, a master dye solution was prepared by dissolving ≈1 mg of Irgalan Black in 1 L of pure water. The master dye was then filtered through a series of Gelman SUPOR filters using a vacuum filtration system with the smallest filter having a pore size of 0.2 μm. The absorbance of the master dye was measured using a 1-cm Starna cell in two separate spectrophotometer systems—an Agilent Cary 6000i (accuracy of 0.0003 absorbance units) and an Agilent 8453 UV-VIS (accuracy of 0.005 absorbance units). The absorbance values varied <1% between the two systems. A plot of the resultant absorption coefficients is shown in Fig. 8.

This master dye was first diluted by a factor of 20 using a 200-mL volumetric flask (measurement uncertainty 0.1%) and a 10-mL graduated pipette (measurement uncertainty 0.2%). The 20× dilution sample was further diluted using a 2-L volumetric flask and a 2-ml graduated pipette (measurement uncertainty 0.1%) to produce 10 reference samples containing different concentrations of dye ranging from $40,000\times$ –$4000\times$. The highest dilution factor ($40,000\times$) was chosen such that the measured dye had an absorption coefficient with the same order of magnitude as the minimum absorption coefficient of water.

The diluted dye samples were loaded into the ICAM-II one by one (from $40,000\times$ to $4000\times$) and measured. S was measured 40 times at each wavelength and averaged. Note, the signal measured was a combination of the dye and the pure water solvent. However, it is assumed that the volume of water, and hence the contribution of the water absorption to the signal, for each diluted dye was constant. Therefore, $\partial\alpha/\partial S$ measured the ICAM-II signal change due to contributions from the dye only.

$\partial\alpha/\partial S$ was calculated by first plotting the values of the absorption coefficient, α_{dye}, measured from the spectrophotometer as a function of the signal, S. A least-squares fit was performed for each wavelength. The slope at each wavelength corresponds to $\partial\alpha/\partial S$ for that wavelength. An example of the fitted slopes is shown in Fig. 9.

These slopes from the dye measurements provided the ICAM-II absorption response, as shown in Fig. 10. The instrument was thoroughly rinsed with 18.2 MΩ · cm water after each measurement.

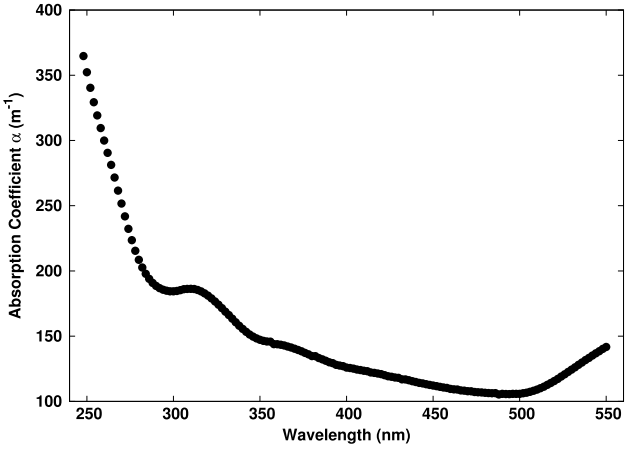

Fig. 8. Absorption spectrum of a 1 mg/L Irgalon Black solution measured by an Aigilent spectrophotometer.

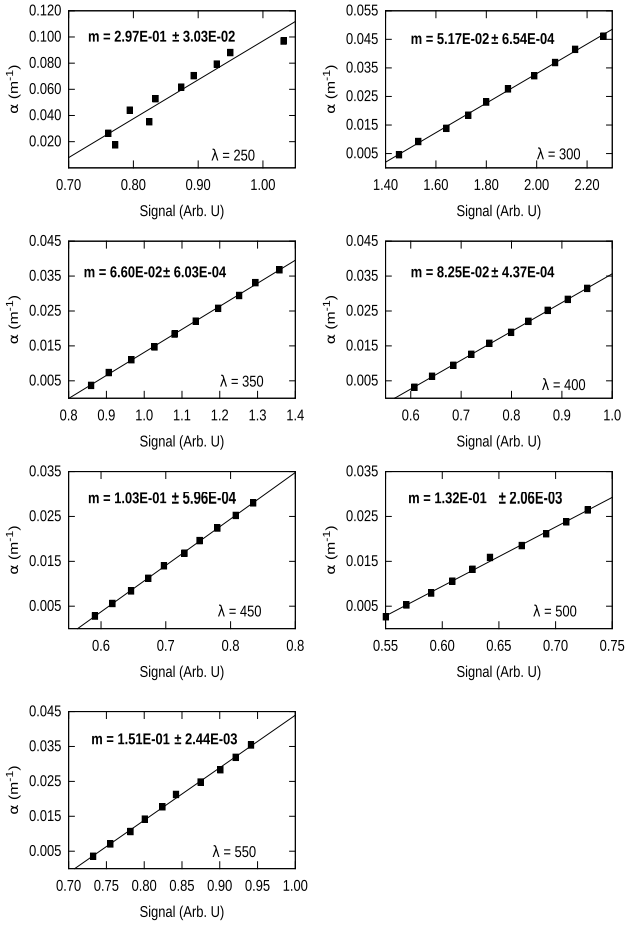

Fig. 9. Absorption coefficient of Irgalon Black as a function of the ICAM-II signal at five of the wavelengths. A least-squares fit was applied at every wavelength.

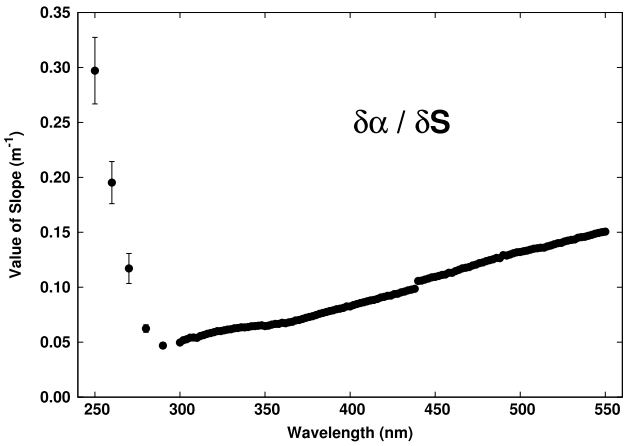

Fig. 10. Measurements of the slopes of the ICAM-II absorption response as a function of wavelength.

D. Absorption Data and Discussion

The absorption spectrum from 250 to 550 nm was calculated for pure water via Eq. (5), i.e., by multiplying the slopes of the ICAM-II spectral response function (Fig. 10) with the slopes of the volumetric function (Fig. 7) and the volume of the sample cell (1538 mL). The results can be seen in Fig. 11. Numerical values for the measured absorption coefficients are shown in Table 2. Data for 310–550 nm were taken at wavelength intervals of 2 nm to reflect the nominal bandwidth of the monochromater (1.8 nm at a slit width of 600 μm). Since the absorption spectrum of pure water is assumed to be smooth, a three-point moving average was applied to the points in this region to help reduce measurement noise. For 250–310 nm, the monochromater slits were widened to allow for better illumination of the ICAM-II. The wavelength intervals were therefore increased to reflect an increase in the nominal bandwidth (6 nm at a slit width of 2000 μm). Since the tail of the first electronic transition centered around 147 nm is predicted to be featureless, no information is lost with the decrease in resolution in the 250–310 nm spectral region [3].

The results in this study shift the wavelength for the minimum absorption of pure water from 418 to 344 nm. Many scientists in the large detector field have already been operating under the assumption that the true minimum of water was found at a wavelength near 350 nm [25]. On the long wavelength side of this minimum, the absorption spectrum, which derives its structure from the vibrational structure of water, behaves exponentially (not accounting for harmonic structure) with a decay constant consistent with other high-quality studies. On the short wavelength side of the minimum, the absorption spectrum (which is dictated by the tail of the first electronic transition) also behaves exponentially.

In previous versions of the ICAM, the volume response and the absorption response were measured by fitting data sets with ≈20 increments in volume and in dye dilutions; this study focused on measuring at a smaller number of increments but with higher accuracy and precision. A single increment for the volume response in the Pope and Fry study used 10–20 averages at a given volume while this study used 100 averages at each increment to further suppress background fluctuations and more reliably detect small contributions [8]. In addition, due to the low irradiance of the cavity at 250 nm, 20 volume increments were measured with 100 averages to help address further noise concerns. As a result, the slopes fitted from the volume response in this study had significantly less error for small absorption coefficient values.

Due to the effectiveness of using a large number of averages during the volume response measurements, a similar approach was taken with the absorption response measurements. Error bars for the final absorption coefficient values of water were calculated using a combination of the standard deviation from several measurements as well as the slope uncertainty from each of the fitted slopes.

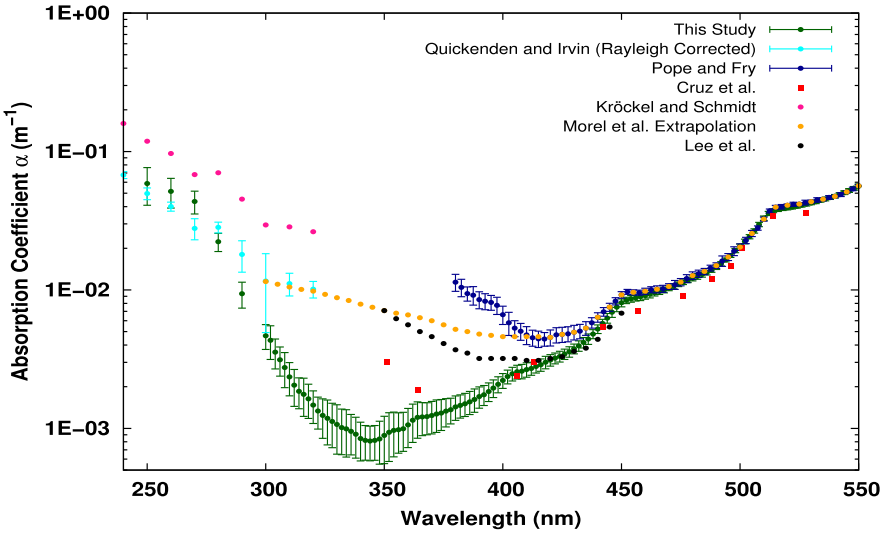

Fig. 11. Absorption coefficient, α, of pure water measured in this study along with the results from several other high-quality studies: Pope and Fry [8], the Rayleigh-scattering-corrected Quickenden and Irvin values [11], Cruz *et al.* [10], Lee *et al.* [30], and Morel *et al.* Extrapolation [17], and data at 10-nm intervals from Kröckel and Schmidt [14].

Table 2. Absorption Coefficients, $\alpha_w(m^{-1})$, and Error, $\sigma(m^{-1})$, for Pure Water as a Function of Wavelength, λ

λ(nm)	$\alpha_w(*10^3)$	$\sigma(*10^3)$	λ(nm)	$\alpha_w(*10^3)$	$\sigma(*10^3)$	λ(nm)	$\alpha_w(*10^3)$	$\sigma(*10^3)$	λ(nm)	$\alpha_w(*10^3)$	$\sigma(*10^3)$
250	58.71	17.79	356	0.98	0.32	422	3.22	0.29	488	13.91	0.49
260	51.50	12.44	358	0.99	0.31	424	3.31	0.29	490	14.60	0.54
270	43.57	8.19	360	1.06	0.33	426	3.44	0.30	492	15.45	0.55
280	22.30	3.34	362	1.15	0.35	428	3.58	0.31	494	16.48	0.54
290	9.39	2.00	364	1.20	0.35	430	3.76	0.31	496	17.74	0.58
300	4.67	0.96	366	1.21	0.32	432	3.95	0.34	498	19.26	0.68
302	4.33	1.18	368	1.22	0.32	434	4.17	0.36	500	20.73	0.74
304	3.56	0.87	370	1.24	0.33	436	4.42	0.38	502	22.42	0.85
306	3.13	0.75	372	1.27	0.34	438	4.80	0.36	504	24.24	0.84
308	2.75	0.78	374	1.29	0.33	440	5.22	0.38	506	26.68	0.96
310	2.36	0.64	376	1.33	0.31	442	5.74	0.40	508	29.71	1.06
312	2.05	0.61	378	1.37	0.29	444	6.26	0.50	510	33.00	1.22
314	1.85	0.47	380	1.43	0.29	446	6.91	0.57	512	35.69	1.23
316	1.76	0.54	382	1.47	0.28	448	7.51	0.55	514	37.38	1.23
318	1.63	0.45	384	1.51	0.29	450	8.08	0.52	516	38.21	1.31
320	1.47	0.39	386	1.55	0.29	452	8.42	0.44	518	38.78	1.29
322	1.33	0.35	388	1.62	0.31	454	8.63	0.48	520	39.17	1.29
324	1.24	0.39	390	1.70	0.30	456	8.77	0.45	522	39.62	1.17
326	1.18	0.42	392	1.75	0.29	458	8.93	0.56	524	40.17	1.22
328	1.12	0.40	394	1.85	0.28	460	9.09	0.52	526	40.88	1.18
330	1.07	0.42	396	1.96	0.28	462	9.33	0.57	528	41.62	1.20
332	1.01	0.37	398	2.08	0.28	464	9.55	0.51	530	42.42	1.17
334	0.99	0.37	400	2.22	0.27	466	9.79	0.51	532	43.30	1.25
336	0.95	0.31	402	2.37	0.27	468	9.99	0.46	534	44.36	1.29
338	0.91	0.30	404	2.48	0.28	470	10.30	0.42	536	45.41	1.40
340	0.85	0.26	406	2.57	0.29	472	10.65	0.45	538	46.45	1.36
342	0.82	0.23	408	2.59	0.31	474	11.00	0.42	540	47.54	1.42
344	0.81	0.23	410	2.66	0.32	476	11.38	0.44	542	48.82	1.41
346	0.82	0.23	412	2.71	0.29	478	11.77	0.46	544	50.40	1.50
348	0.84	0.29	414	2.80	0.29	480	12.14	0.52	546	52.24	1.50
350	0.89	0.33	416	2.88	0.30	482	12.54	0.60	548	54.25	1.63
352	0.94	0.36	418	3.00	0.31	484	12.94	0.55	550	56.29	1.84
354	0.97	0.34	420	3.12	0.30	486	13.36	0.53			

The absorption coefficient of pure water is greatly influenced by three distinct factors for wavelengths <400 nm. First, ultraviolet absorption measurements are particularly sensitive to organic contamination. Nucleic acids have a strong absorption peak centered around 260 nm with a tail that continues far into the longer wavelengths of the ultraviolet [26]. As a result, a sample with a small number of organics can overestimate the absorption coefficient of that sample, particularly when the sample absorption is weak. The organic content of the water in this study is consistent with the exceptional water quality of the most recent studies (3–5 ppb). Second, Heidt, and Johnson (1951) have shown that dissolved oxygen can increase the measured absorption. Quickenden and Irvin introduced many exhaustive steps to remove dissolved oxygen [27]. However, Kröckel and Schmidt demonstrated that many state-of-the-art, commercially available water systems are capable of producing water with levels of dissolved oxygen comparable to those of Quickenden and Irvin. While reproducing the attenuation results of Quickenden and Irvin, Krockel and Schmidt noted that "an additional cleaning step with a double distill under nitrogen atmosphere did not change the lab analysis nor the UV spectra of our water" [14]. This is consistent with the results of this study which observed that additional bubbling of N_2 and Ar through the Milli-Q water had no impact on the absorption spectrum. Furthermore, since the minimum absorption in this study is much lower than any other well-regarded study, the hypothesis that dissolved oxygen impacts this study is likely implausible as it would cause the absorption to be larger, not smaller, than the previous studies. Finally, several studies have demonstrated a redshift in the ultraviolet absorption spectrum due to temperature [28]. While a detailed temperature

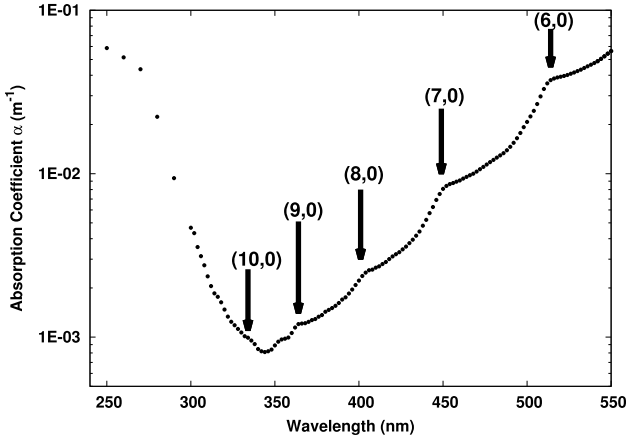

Fig. 12. Present results for pure water. (n, 0) denotes the nth harmonic of the pure O–H stretch (no scissor mode combination). A large arrow is used to show the predicted locations of those harmonics.

investigation is outside the scope of this study, we note that the water was measured at a temperature of 23 ± 0.5°C.

The results in this study agree with the Rayleigh-corrected values of the Quickenden and Irvin [11] and the Kröckel and Schmidt [14] studies from 250 to 300 nm (within error bars). However, for $\lambda > 300$ nm, the data from the many high-quality studies diverges from the data obtained using ICAM-II. As highlighted in the introduction to this study, these studies measured the attenuation of a pure water sample, not the absorption. The absorption was obtained after applying a scattering correction based on calculations from the best scattering parameters. This problem is sufficiently highlighted when comparing the Quickenden and Irvin study with the Kröckel and Schmidt study. While both studies measure the same attenuation, the studies disagree on the absorption. Furthermore, if the scattering is much larger than the absorption, subtle absorption features can be obfuscated by the overwhelming scattering losses. These problems are eliminated with a scattering-independent measurement like the ICAM-II.

Similarly, the final results are in excellent agreement with Pope and Fry for wavelengths >440 nm [8]. Figure 12 shows the present results for pure water absorption with the locations of several harmonics from the O–H stretch. Resonances from the seventh and eighth harmonics of the O–H stretch that are consistent with previous efforts are still visible [29]. In fact, these data demonstrate the first known observation of the ninth harmonic of the O–H stretch. This appears as a small feature at 364 nm which was predicted by Tam and Patel in the equation

$$\nu_n = n(3620 - 63n)\text{cm}^{-1}, \quad (6)$$

where n denotes harmonic order. However, the results from the Pope and Fry study suggest that the absorption of water begins to increase below 420 nm. Recall that the original ICAM was made with Spectralon, which, in addition to having a lower reflectivity, will absorb UV radiation and even degrade under long-term exposure [16]. Since the light in an integrating cavity actually penetrates the wall a short distance, absorption by the wall material will look like the sample is absorbing (i.e., α does not affect, but is included in). Consequently, this increased absorption of Spectralon can cause an overestimation of the sample absorption coefficient. Since fumed silica does not begin to significantly absorb until $\lambda < 250$ nm, the ICAM-II is better suited to measure samples between 250 and 400 nm.

The absorption spectrum of "pure" seawater as measured by Lee *et al.* was included in Fig. 11. The absorption coefficients measured by Lee *et al.* were higher than the results in this study for $\lambda < 400$ nm. This difference is not surprising since the "pure" seawater used by Lee *et al.* was likely less pure than the laboratory-grade pure water used in this study [30]. The results from Lee *et al.* still serve as an accurate representation of the absorption spectrum of the clearest natural waters.

We finally compare the recent results in this study with the results of Cruz *et al.* The Cruz *et al.* results were met with some skepticism for two reasons: (i) they lacked an additional step to remove dissolved oxygen from the water produced by the Milli-Q system and (ii) they differed from the well-established studies. Since this study uses the same Milli-Q purification system as Cruz *et al.*, the dissolved oxygen discussion in this paper applies to their study as well. The results in this study agree remarkably well with Cruz *et al.* for 400 nm $< \lambda <$ 450 nm and $\lambda > 500$ nm. The difference between the two studies at 350 nm may be the result of an unaccounted loss due to scattering effects [10].

E. Summary

A comprehensive spectrum of water from 250 to 550 nm has been presented. The data provides the first scattering-independent measurement for wavelengths between the electronic transition region in the UV and the molecular vibration region in the VIS-NIR. This study demonstrates a minimum absorption of water at a wavelength that is much lower (≈345 nm) than previously understood (≈420 nm). The ICAM-II demonstrates effectiveness in measuring weak optical absorption to a high accuracy and provides the most reliable data for water at 23°C from 250 to 550 nm.

Funding. National Science Foundation (NSF) (OCE-1333425); George P. Mitchell Chair in Experimental Physics.

Acknowledgment. The authors thank Bill Merka for his assistance in maintaining and preparing glassware. The authors acknowledge the contributions of the reviewers whose questions and comments greatly assisted in the presentation of this work. Specifically, we acknowledge Dr. Mike Twardowski for his thoughtful discussions and excellent insights that helped to tackle this complex problem.

REFERENCES

1. Z. P. Lee, K. L. Carder, and R. A. Arnone, "Deriving inherent optical properties from water color: a multiband quasi-analytical algorithm for optically deep waters," Appl. Opt. **41**, 5755–5772 (2002).
2. B. Wozniak and J. Dera, *Light Absorption in Sea Water* (Springer, 2007).
3. M. Jonasz and G. Fournier, *Light Scattering by Particles in Water: Theoretical and Experimental Foundations* (Academic, 2011).
4. R. W. Preisendorfer, *Hydrological Optics* (NOAA, 1976), Vol. **1**.
5. J. E. Cloern, "The relative importance of light and nutrient limitation of phytoplankton growth: a simple index of coastal ecosystem sensitivity to nutrient enrichment," Aquat. Ecol. **33**, 3–15 (1999).
6. R. J. Cogdell, "Carotenoids in photosynthesis," Philos. Trans. R. Soc. B **284**, 569–579 (1978).
7. M. R. Querry, D. M. Wieliczka, and D. J. Segelstein, "Water (H_2O)," in *Handbook of Optical Constants of Solids II* (Academic, 1991), pp. 1059–1077.
8. R. M. Pope and E. S. Fry, "Absorption spectrum (380–700 nm) of pure water. II. Integrating cavity measurements," Appl. Opt. **36**, 8710–8723 (1997).
9. F. M. Sogandares, "The spectral absorption of pure water," Ph.D. thesis (Texas A&M University, 1991).
10. R. A. Cruz, A. Marcano, C. Jacinto, and T. Catunda, "Ultrasensitive thermal lens spectroscopy of water," Opt. Lett. **34**, 1882–1884 (2009).
11. T. I. Quickenden and J. A. Irvin, "The ultraviolet absorption spectrum of liquid water," J. Chem. Phys. **72**, 4416–4428 (1980).
12. E. S. Fry, "Visible and near-ultraviolet absorption spectrum of liquid water: comment," Appl. Opt. **39**, 2743–2744 (2000).
13. J. A. Ghormley and C. J. Hochanadel, "Production of hydrogen, hydroxide, and hydrogen peroxide in the flash photolysis of ice," J. Phys. Chem. **75**, 40–44 (1971).
14. L. Kröckel and M. A. Schmidt, "Extinction properties of ultrapure water down to deep ultraviolet wavelengths," Opt. Mater. Express **4**, 1932–1942 (2014).
15. E. S. Fry, G. W. Kattawar, and R. M. Pope, "Integrating cavity absorption meter," Appl. Opt. **31**, 2055–2065 (1992).

16. “A guide to reflectance coatings and materials,” Technical Report (Labsphere, 2015).
17. A. Morel, B. Gentili, H. Claustre, M. Babin, A. Bricaud, J. Ras, and F. Tieche, “Optical properties of the ‘clearest’ natural waters,” Limnol. Oceanogr. **52**, 217–229 (2007).
18. M. T. Cone, J. A. Musser, E. Figueroa, J. D. Mason, and E. S. Fry, “Diffuse reflecting material for integrating cavity spectroscopy, including ring-down spectroscopy,” Appl. Opt. **54**, 334–346 (2015).
19. J. N. Bixler, M. T. Cone, B. H. Hokr, J. D. Mason, E. Figueroa, E. S. Fry, V. V. Yakovlev, and M. O. Scully, “Ultrasensitive detection of waste products in water using fluorescence emission cavity-enhanced spectroscopy,” Proc. Natl. Acad. Sci. USA **111**, 7208–7211 (2014).
20. M. T. Cone, J. D. Mason, E. Figueroa, B. H. Hokr, J. N. Bixler, C. C. Castellanos, G. D. Noojin, J. C. Wigle, B. A. Rockwell, V. V. Yakovlev, and E. S. Fry, “Measuring the absorption coefficient of biological materials using integrating cavity ring-down spectroscopy,” Optica **2**, 162–168 (2015).
21. ET Enterprises Ltd., “51 mm (2″) photomultiplier, 9813B series data sheet,” Technical Report (Electron Tubes, 2015).
22. E. Millipore, “Milli-Q water purification systems range,” Technical Report (Millipore, 2016).
23. I. B. Butler, M. A. Schoonen, and D. T. Rickard, “Removal of dissolved oxygen from water: a comparison of four common techniques,” Talanta **41**, 211–215 (1994).
24. T. Ohmi, A. Hogetsu, K. Ushikoshi, and M. Saito, “Ultrapure water producing system,” U.S. patent 5,124,033 (30 April 1992).
25. K. Abe, Y. Hayato, T. Iida, M. Ikeda, C. Ishihara, K. Iyogi, J. Kameda, K. Kobayashi, Y. Koshio, and Y. Kozuma, “Solar neutrino results in Super-Kamiokande-III,” Phys. Rev. D **83**, 052010 (2011).
26. A. V. Tataurov, Y. You, and R. Owczarzy, “Predicting ultraviolet spectrum of single stranded and double stranded deoxyribonucleic acids,” J. Biophys. Chem. **133**, 66–70 (2008).
27. L. J. Heidt and A. M. Johnson, “Optical study of the hydrates of molecular oxygen in water,” J. Am. Chem. Soc. **79**, 5587–5593 (1957).
28. O. Ryumyo and T. Takahashi, “Vacuum uv absorption spectra of liquid water and ice,” J. Phys. Soc. Jpn. **24**, 548–550 (1968).
29. C. Patel and A. Tam, “Optical absorption coefficients of water,” Nature **280**, 302–304 (1979).
30. Z. Lee, J. Wei, K. Voss, M. Lewis, A. Bricaud, and Y. Huot, “Hyperspectral absorption coefficient of ‘pure’ seawater in the range of 350–550 nm inverted from remote sensing reflectance,” Appl. Opt. **54**, 546–558 (2015).